

Mass-independent isotopic fractionation: Recent developments

Subrata Chakraborty* and S. K. Bhattacharya

Physical Research Laboratory, Ahmedabad 380 009, India

It has been about three decades since the discovery of anomalous (mass-independent) oxygen isotopic composition in meteoritic materials. Since then, mass-independent oxygen isotopic compositions have been observed in a number of stratospheric species like ozone. A significant amount of experimental as well as theoretical work has been carried out to understand the origin of mass-independent fractionation. In recent years, there has been notable progress in gaining insight into some of these processes through precise stratospheric observations, new kinds of laboratory experiments and theoretical models. In this article we present the recent developments in this field of research.

THE partitioning of isotopes of an element which is distributed into two or more phases by different physico-chemical processes is called isotopic fractionation. There are two major classes of processes: (i) isotopic exchange reactions (equilibrium process) and (ii) kinetic processes (such as diffusion, condensation, evaporation, etc.) responsible for isotopic fractionation in nature¹. The theoretical basis for estimating the magnitude of fractionation for each of these processes differs, but the underlying principle for each is that the effects are dependent on mass. A fractionation process can be comprehensively studied if it involves an element with three or more isotopes. The best examples are oxygen (¹⁶O, ¹⁷O and ¹⁸O), sulphur (³²S, ³³S, ³⁴S, ³⁶S) and magnesium (²⁴Mg, ²⁵Mg, ²⁶Mg).

The simple rule of mass-dependent isotopic fractionation for three oxygen isotopes (¹⁶O, ¹⁷O and ¹⁸O) (assuming a linear relationship) is,

$$\delta^{17}\text{O} = \beta(\delta^{18}\text{O}). \quad (1)$$

The calculated β is slightly more than half (ranging from 0.51 to 0.52 depending upon the particular process involved)¹ and (1) is generally written as,

$$\delta^{17}\text{O} = 0.52(\delta^{18}\text{O}). \quad (2)$$

Experimentally, the oxygen isotopic compositions of most of the terrestrial, lunar and some meteoritic materials lie on a line with a slope ~ 0.5 in a three-isotope plot as shown in Figure 1.

Though rare, there are processes in nature which do not follow the above mass-dependent fractionation rule.

These processes display mass-independent or nonmass-dependent isotopic fractionation. For oxygen isotopes, the mass-independent fractionation is readily apparent when,

$$\delta^{17}\text{O} \neq 0.52(\delta^{18}\text{O}). \quad (3)$$

The degree of mass-independent fractionation is measured by

$$\Delta^{17}\text{O} = \delta^{17}\text{O} - 0.52(\delta^{18}\text{O}). \quad (4)$$

There are two natural systems where mass-independent oxygen isotopic fractionations have been observed^{2,3}. First, 'the early solar system' archive, where the mass-independent oxygen isotopic compositions have been discovered in a number of oxide grains from different meteorites⁴⁻⁷. Second, the oxygen-containing gaseous species (such as ozone, CO₂, CO and N₂O) of the earth's atmosphere carry mass-independent signatures⁸⁻¹⁹. In the present article, we will constrain the discussion to ozone and CO₂.

Equations (1)–(4) outlined above are derived from the basic power law of fractionation involving fractionation factor α : $\alpha_{17/16} = (\alpha_{18/16})^\beta$, assuming linear relationship. In a recent publication²⁰ these relations are presented in more accurate form, which shows that the nonlinearity is severe for cases where the sample data set includes points of large $|\delta^{17}\text{O}|$ and $|\delta^{18}\text{O}|$. These nonlinear expressions are important for interpreting the data set, where the isotopic compositions marginally deviate from the terrestrial silicate composition (as for example, in case of atmospheric oxygen). Moreover, in the case of oxygen from extraterrestrial reservoirs, where the mass-dependent fractionation line may be parallel to that of the bulk silicate Earth but away from it, an extra term is necessary in the above-mentioned equation to quantify the offset²⁰. However, the present article will not use any of these nonlinear relationships to interpret the existing data on ozone or carbon dioxide.

Ozone formation mechanism

According to the Chapman mechanism, stratospheric ozone is formed through photolysis of oxygen below 185 nm followed by third body recombination of ground state O-atoms with O₂ molecules to form O₃.

*For correspondence. (e-mail: subrata@prl.ernet.in)

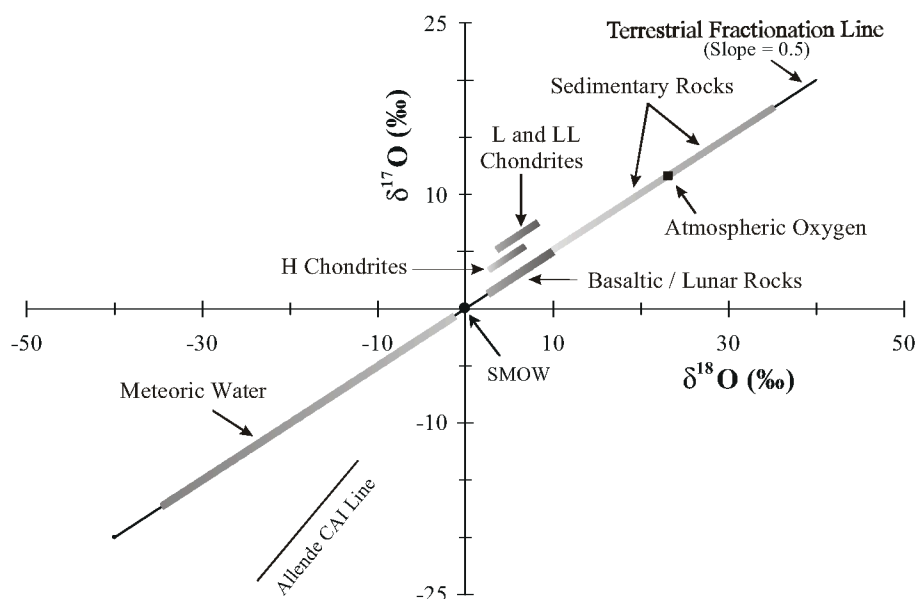
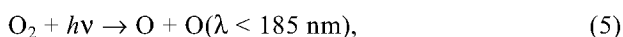


Figure 1. Three-isotope plot of oxygen isotopic compositions of various terrestrial materials, which define a mass-dependent fractionation line known as terrestrial mass fractionation line. Along with the Allende CAI line, the compositions of three classes of chondritic meteorites (L, LL and H) and the lunar rocks are shown. SMOW represents standard mean ocean water, a reference for all oxygen isotopic measurements.



The photo-dissociation coefficient of eq. (5) is $1.2 \times 10^{-12}/\text{s}$ in the Earth's atmosphere at 25 km, and the rate coefficient of eq. (6) is $6 \times 10^{-34} \text{ cm}^3 \text{ mol}^{-1} \text{ s}^{-1}$ (at 300 K). Ozone so formed is dissociated by visible and UV wavelengths and by O atoms,



The photo-dissociation coefficient of eq. (7) is $2.1 \times 10^{-4}/\text{s}$ in the Earth's atmosphere at 25 km, and the rate coefficient of eq. (8) is $8 \times 10^{-15} \text{ cm}^3 \text{ mol}^{-1} \text{ s}^{-1}$ (at 298 K). The photo-dissociation coefficients and rate constants are from DeMore *et al.*²¹.

Oxygen isotopic enrichment in stratospheric ozone

Two types of techniques have been employed for oxygen isotopic measurements in stratosphere ozone: the mass-spectrometric methods (*in situ* and return-sample measurement) and the spectroscopic methods. Anderson *et al.*²² summarized the stratospheric measurements performed before 1995 by both the techniques.

Recently, Krankowsky *et al.*¹² measured the O_3 isotopic composition (with reasonably good precision) of a large number of stratospheric samples collected by four

different balloon flights during 1998–2000 within the altitude range of 22 to 33 km using a modified cryogenic sample-collector system²³. The balloon flights were conducted from Aire-sur-l'Adour, France and Kiruna, Sweden. The enrichment variation was found to be within 70 to 110‰ in $^{50}\text{O}_3$. None of the samples showed the very high level of enrichment ($\sim 400\%$) observed by Mauersberger⁸. The observed maximum enrichment value in $^{49}\text{O}_3$ was about 95‰ (with a range of 68 to 95‰). Based on the recent measurements, Mauersberger *et al.*¹⁰ sorted out the acceptable data from the previous measurements and discarded the higher values observed earlier on technical ground. The most recent measurements of collected samples by Lämmerzahl *et al.*²⁴ from eight balloon flights from the same places at different times of the year (following the same procedure) confirm the new database of stratospheric measurements. It is now evident from these new data sets that the enrichments in the two heavy isotopomers of ozone ($^{49}\text{O}_3$ and $^{50}\text{O}_3$) are linearly correlated with a slope ($\Delta\delta^{17}\text{O}/\Delta\delta^{18}\text{O}$) value of 0.62.

Laboratory studies

Ozone formation

Thiemens and Heidenreich²⁵ demonstrated for the first time that a chemical process could generate mass-independent isotopic fractionation. In that important experiment, ozone formed from molecular oxygen showed extremely enriched oxygen isotopic composition with $\delta^{17}\text{O} = \delta^{18}\text{O}$ instead of $\delta^{17}\text{O} = 0.52\delta^{18}\text{O}$. In the last three

decades, several laboratory studies have been performed by different groups for understanding the anomalous isotopic enrichment in ozone. These studies include pressure and temperature dependence of enrichment^{26–29}, and show that at around 10 torr of oxygen pressure, the enrichment in $^{50}\text{O}_3$ is about 130%, while the enrichment in $^{49}\text{O}_3$ is 110%. The enrichments decrease above 50 torr and diminish to a low level of 30% at 10 atm. Also, the isotopic enrichment in both the isotopomers reduces with decreasing temperature. In a more advanced experiment, Mauersberger *et al.*³⁰ formed ozone by $\text{O} + \text{O}_2$ recombination with isotopic variants of the atom and molecule in their ground electronic states to study the distribution of all possible ozone isotopomers. Results show that with respect to $^{48}\text{O}_3$ ($^{16}\text{O}^{16}\text{O}^{16}\text{O}$), the two symmetric isotopomers $^{17}\text{O}^{17}\text{O}^{17}\text{O}$ and $^{18}\text{O}^{18}\text{O}^{18}\text{O}$ were depleted. A large enrichment of about 180% was found in the most asymmetric isotopomer $^{16}\text{O}^{17}\text{O}^{18}\text{O}$, while all other asymmetric isotopomers carry enrichment of about two-third this value. The importance of this experiment was in establishing the connection between the enrichment and the symmetry of the ozone molecule. A detailed discussion on all these previous experimental studies can be found in Anderson *et al.*²².

To gain further insight into the process responsible for isotopic enrichment in ozone, relative rate coefficients of different isotopomer forming channels were determined^{31–34} (see Table 1). These data illustrate the importance of symmetry and change in zero point energy (ZPE) associated with these reactions. For example, the heteronuclear oxygen reactions (10) and (11) for the same isotopomer of mass 50 ($^{18}\text{O}^{16}\text{O}^{16}\text{O}$ and $^{16}\text{O}^{18}\text{O}^{16}\text{O}$) show a pronounced difference in the formation rates of the symmetric and asymmetric species (1.45 and 1.08 respectively). These two are exclusively responsible for the enrichment in $^{50}\text{O}_3$, making an overall rate of 1.27 for the $^{16}\text{O} + ^{16}\text{O}^{18}\text{O}$ channel³³. The importance of ZPE change has been explained in detail by Janssen *et al.*³⁴ who show that the relative rate coefficient is approximately linearly related to ΔZPE , where ΔZPE denotes the difference in ZPE of oxygen molecules of the corresponding isotope exchange reactions. The calculation shows that isotope exchange reaction corresponding to the channel (24) has the highest ΔZPE (23 cm^{-1}) corresponding to the highest relative rate coefficient of 1.50.

The rate constant investigation is still not complete. Specifically, investigations involving the rare isotope ^{17}O distribution (which make the experiments more challenging) in ozone isotopomers have to be carried out.

Ozone dissociation

Ozone dissociation is an integral part of the chain of processes during ozone formation by UV photolysis of oxygen as obvious from the reaction chain described by

Table 1. Reaction channels of all possible oxygen combinations leading to ozone molecules with exit channel-specific rate coefficient. Rate coefficients are relative to the standard rate for $^{16}\text{O} + ^{16}\text{O}^{18}\text{O} + \text{M}$ of $6.05 \times 10^{-34}\text{ cm}^6\text{ s}^{-1}$ (after Janssen *et al.*³⁴)

Mass	Reaction channel no.	Reaction	Relative rate coefficient
48	1	$^{16}\text{O} + ^{16}\text{O}^{16}\text{O} \rightarrow ^{16}\text{O}^{16}\text{O}^{16}\text{O}$	1.00
49	2	$^{16}\text{O} + ^{16}\text{O}^{17}\text{O} \rightarrow ^{16}\text{O}^{16}\text{O}^{17}\text{O}$	
	3	$\rightarrow ^{16}\text{O}^{17}\text{O}^{16}\text{O}$	
	4	$^{17}\text{O} + ^{16}\text{O}^{16}\text{O} \rightarrow ^{17}\text{O}^{16}\text{O}^{16}\text{O}$	1.03
	5	$\rightarrow ^{16}\text{O}^{17}\text{O}^{16}\text{O}$	
50	6	$^{16}\text{O} + ^{17}\text{O}^{17}\text{O} \rightarrow ^{16}\text{O}^{17}\text{O}^{17}\text{O}$	1.23
	7	$\rightarrow ^{17}\text{O}^{16}\text{O}^{17}\text{O}$	
	8	$^{17}\text{O} + ^{16}\text{O}^{17}\text{O} \rightarrow ^{17}\text{O}^{16}\text{O}^{17}\text{O}$	
	9	$\rightarrow ^{17}\text{O}^{17}\text{O}^{16}\text{O}$	
	10	$^{16}\text{O} + ^{16}\text{O}^{18}\text{O} \rightarrow ^{16}\text{O}^{16}\text{O}^{18}\text{O}$	1.45
	11	$\rightarrow ^{16}\text{O}^{18}\text{O}^{16}\text{O}$	1.08
	12	$^{18}\text{O} + ^{16}\text{O}^{16}\text{O} \rightarrow ^{18}\text{O}^{16}\text{O}^{16}\text{O}$	0.92
	13	$\rightarrow ^{16}\text{O}^{18}\text{O}^{16}\text{O}$	0.006
51	14	$^{17}\text{O} + ^{17}\text{O}^{17}\text{O} \rightarrow ^{17}\text{O}^{17}\text{O}^{17}\text{O}$	1.02
	15	$^{16}\text{O} + ^{17}\text{O}^{18}\text{O} \rightarrow ^{16}\text{O}^{17}\text{O}^{18}\text{O}$	
	16	$\rightarrow ^{16}\text{O}^{18}\text{O}^{17}\text{O}$	
	17	$\rightarrow ^{17}\text{O}^{16}\text{O}^{18}\text{O}$	
	18	$^{17}\text{O} + ^{16}\text{O}^{18}\text{O} \rightarrow ^{17}\text{O}^{16}\text{O}^{18}\text{O}$	
	19	$\rightarrow ^{17}\text{O}^{18}\text{O}^{16}\text{O}$	
	20	$\rightarrow ^{16}\text{O}^{17}\text{O}^{18}\text{O}$	
	21	$^{18}\text{O} + ^{16}\text{O}^{17}\text{O} \rightarrow ^{18}\text{O}^{16}\text{O}^{17}\text{O}$	
	22	$\rightarrow ^{18}\text{O}^{17}\text{O}^{16}\text{O}$	
	23	$\rightarrow ^{16}\text{O}^{18}\text{O}^{17}\text{O}$	
52	24	$^{16}\text{O} + ^{18}\text{O}^{18}\text{O} \rightarrow ^{16}\text{O}^{18}\text{O}^{18}\text{O}$	1.50
	25	$\rightarrow ^{18}\text{O}^{16}\text{O}^{18}\text{O}$	0.029
	26	$^{18}\text{O} + ^{16}\text{O}^{18}\text{O} \rightarrow ^{18}\text{O}^{16}\text{O}^{18}\text{O}$	1.04
	27	$\rightarrow ^{18}\text{O}^{18}\text{O}^{16}\text{O}$	0.92
	28	$^{17}\text{O} + ^{17}\text{O}^{18}\text{O} \rightarrow ^{17}\text{O}^{17}\text{O}^{18}\text{O}$	
	29	$\rightarrow ^{17}\text{O}^{18}\text{O}^{17}\text{O}$	
	30	$^{18}\text{O} + ^{17}\text{O}^{17}\text{O} \rightarrow ^{18}\text{O}^{17}\text{O}^{17}\text{O}$	1.03
	31	$\rightarrow ^{17}\text{O}^{18}\text{O}^{17}\text{O}$	
53	32	$^{17}\text{O} + ^{18}\text{O}^{18}\text{O} \rightarrow ^{17}\text{O}^{18}\text{O}^{18}\text{O}$	1.31
	33	$\rightarrow ^{18}\text{O}^{17}\text{O}^{18}\text{O}$	
	34	$^{18}\text{O} + ^{17}\text{O}^{18}\text{O} \rightarrow ^{18}\text{O}^{17}\text{O}^{18}\text{O}$	
	35	$\rightarrow ^{18}\text{O}^{18}\text{O}^{17}\text{O}$	
54	36	$^{18}\text{O} + ^{18}\text{O}^{18}\text{O} \rightarrow ^{18}\text{O}^{18}\text{O}^{18}\text{O}$	1.03

eqs (5)–(8). Therefore, in addressing the issue of isotopic enrichment in ozone (as described in the previous section), it is important to characterize its different dissociation channels. The relevant dissociation pathways are: (i) photo-dissociation, (ii) thermal dissociation, (iii) dissociation by chemical reactions, and (iv) dissociation through surface interaction³⁵. Among these four pathways, thermal dissociation was studied in detail by Wen and Thiemens^{36,37} and Kim and Yang³⁸. Their studies show some intriguing aspects during ozone dissociation in gaseous phase. Below 90°C , thermally dissociated ozone yields isotopically light oxygen and the left-over ozone is enriched in a mass-dependent fashion. Above 90°C , the isotopic behaviour flips and the product oxygen becomes heavier in a mass-independent fashion. However, enrichment of the oxygen formed in ozone dissociation is substantially less than that for the ozone formed from the oxygen.

Dissociation of ozone by reaction with NO_2 was studied recently by Chakraborty and Thiemens (pers. commun.). The left-over ozone shows a normal mass-dependent enrichment, as seen in most of the chemical reactions.

Among the other two dissociation pathways, two earlier studies dealt with photo-dissociation of ozone by UV and visible light^{37,39}, which showed slight deviation from mass dependence in the case of UV dissociation. In the following section, we will discuss the present understanding about photo-dissociation and surface-induced dissociation of ozone.

The photo-dissociation of ozone produces isotopically light oxygen and as a consequence the left-over ozone becomes heavier. However, the fractionation pattern is not similar in visible and UV wavelengths. In the visible range it is strictly mass-dependent ($\Delta\delta^{17}\text{O}/\Delta\delta^{18}\text{O} = 0.54$), whereas in the UV region it shows deviation from mass dependency ($\Delta\delta^{17}\text{O}/\Delta\delta^{18}\text{O} = 0.63$, Figure 2, after Chakraborty and Bhattacharya⁴⁰). In a critical analysis, it was seen that the product O-atom in reaction eq. (7) is in the excited state ($\text{O}(^1\text{D})$) for higher photon energy ($\lambda < 310 \text{ nm}$), and for lower photon energies ($\lambda > 310 \text{ nm}$), the product O-atom is in ground state ($\text{O}(^3\text{P})$) (ref. 41). The reaction rate coefficient of eq. (8) is comparatively very high ($1.1 \times 10^{-10} \text{ cm}^3/\text{mol/s}$ at 298 K)²¹ when the participating O-atom is in the $\text{O}(^1\text{D})$ state compared to when the participating O-atom is in the $\text{O}(^3\text{P})$ state ($8.0 \times 10^{-15} \text{ cm}^3/\text{mol/sec}$ at 298 K)²¹. Therefore, in

general, photo-dissociation in the UV range involves both reactions (7) and (8), whereas in visible wavelengths only reaction (7) takes place. Reactions (7) and (8) have been decoupled for UV range photo-dissociation in a recent experiment⁴⁰. Knowing the fact that N_2 quenches $\text{O}(^1\text{D})$ quite efficiently ($2.6 \times 10^{-11} \text{ cm}^3/\text{mol/s}$ at 298 K)²¹, O_3 photo-dissociation was carried out with a Hg resonance lamp in the presence of N_2 at different partial pressures. It is noted that at lower N_2 pressure, the slope is 0.63 as observed for UV range photo-dissociation, but with increasing N_2 pressure, the slope gradually increases and reaches a saturation value of unity. It is interpreted by the authors that at higher N_2 pressure, quenching of $\text{O}(^1\text{D})$ by N_2 is more efficient compared to quenching by O_3 , and, therefore, the follow-up reaction (8) cannot take place. Therefore, the change in slope reflects that *pure UV photo-dissociation* (reaction (7)) is a mass-independent process, which proceeds with a slope ($\Delta\delta^{17}\text{O}/\Delta\delta^{18}\text{O}$) value of unity. In contrast, reaction (8) has the property of a normal chemical reaction and these two reactions (7) and (8) together give rise to the deviation from mass dependency during UV photo-dissociation.

An interesting feature has recently been discovered during ozone dissociation induced by a surface^{35,42}. It is seen that dissociation yields isotopically light oxygen and the left-over ozone gets enriched in a mass-independent fashion.

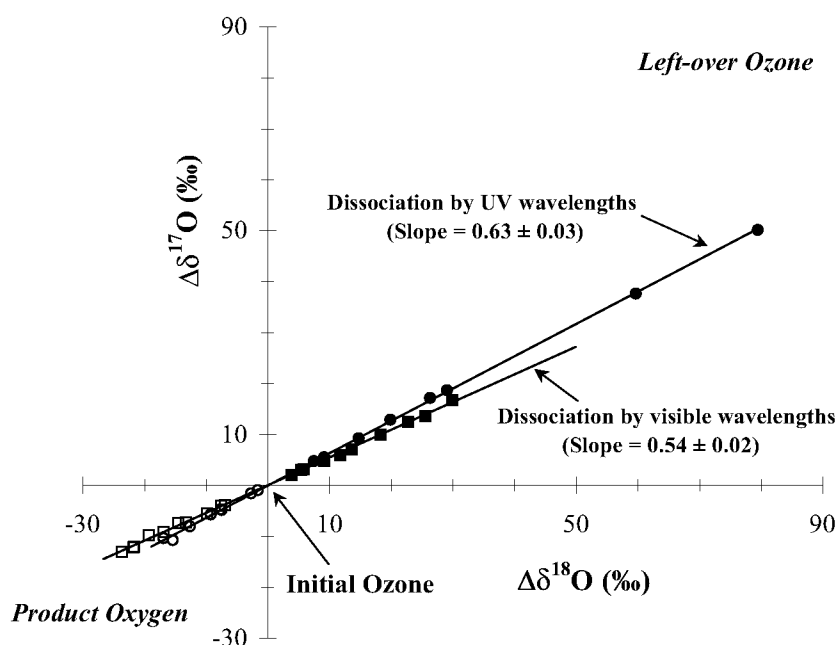


Figure 2. Covariation plot between $\Delta\delta^{17}\text{O}$ and $\Delta\delta^{18}\text{O}$ for photo-dissociation of ozone in UV (circles) and visible wavelengths (squares). The left-over ozone (filled symbols) is enriched and the product oxygen (unfilled symbols) is depleted with respect to the initial ozone. The best-fit line for the visible light dissociation gives a slope of 0.54 ± 0.02 indicating a mass-dependent process, while the UV dissociation gives a slope of 0.63 ± 0.03 reflecting slight deviation from mass dependency (after Chakraborty and Bhattacharya⁴⁰).

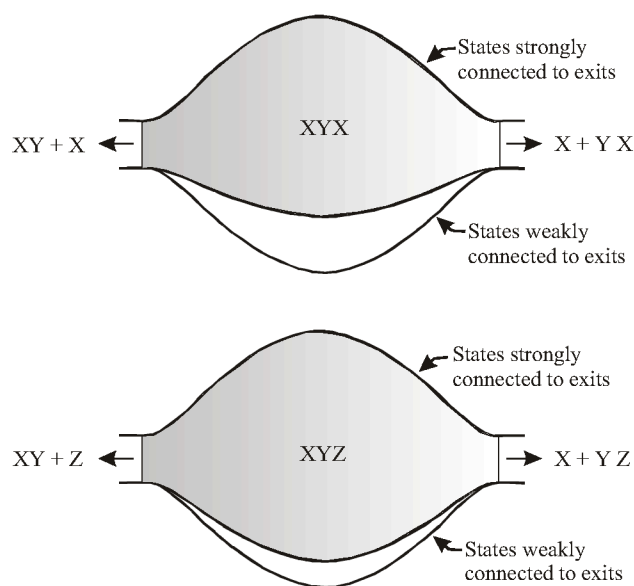


Figure 3. Schematic diagram for ozone molecules of type XYX and XYZ showing differences in proportion of rotational-vibrational states of ozone strongly coupled (shaded region) to the two dissociation exit channels of ozone and those that are weakly coupled (unshaded region) to the exit channels (after Gao and Marcus⁵²).

Altitudinal variation of ^{18}O enrichment in ozone: A topic of debate

Though it is firmly established that ozone in the stratosphere is isotopically enriched, the nature of the variation of enrichment with altitude is not clear. Since the ozone concentration is only about 30 ppb at the stratospheric peak, the isotopic measurements are difficult and have comparatively large uncertainties. It is apparent from the recent database (of mass-spectrometric measurements) that isotopic enrichment increases with altitude, initially slowly but sharply above 30 km. Unfortunately, no high-precision mass-spectrometric data exist above 33 km.

By spectroscopic measurement, Irion *et al.*⁴³ reported integrated enrichment in $^{50}\text{O}_3$ of 130‰ (with large error of 50‰) between 25 and 41 km based on ATMOS Infrared solar spectra and at the same time, Meier and Notholt⁴⁴ reported a similar level of enrichment with smaller error. Since the average of these measurements itself is 130‰, it is expected that much higher level of enrichment would prevail at altitudes beyond 30 km, taking mass-spectrometric values¹⁰ at the lower level as representative.

Krankowsky *et al.*¹² and Mauersberger *et al.*¹⁰ attempted to explain the altitude variations in ozone isotopic enrichments through temperature dependence. In the stratosphere, as one goes up, the temperature increases from about 217.6 to about 231 K, within the altitude range of 21 to 33 km. It is surmised that since the enrichment increases with increase in temperature, as observed by Morton *et al.*²⁹, the stratospheric temperature

increase can account for the altitude variation. However, the average temperature coefficient is only 0.6‰ per K (ref. 29) and this can result in an increase of about 8‰, which is far too small compared to the observed increase of about 30‰. Therefore, Bhattacharya *et al.*⁴⁵ argued that the temperature is not the sole cause of observed increase in enrichment. Through a set of laboratory experiments, they demonstrated that significant enrichments could be obtained if formation and dissociation are allowed to proceed during ozone formation in lower oxygen pressure ranges (< 50 torr). Interestingly, they observed that enrichment in ozone increases with lowering of pressure and they proved that this effect is due to ozone dissociation. To incorporate the dissociation effect in enrichment, they defined a parameter called turn-over time ($\tau = [\text{O}_3]/d[\text{O}_3]/dt$, where $[\text{O}_3]$ is the ozone amount at a given time and $d[\text{O}_3]/dt$ is the dissociation rate at that time) of the ozone reservoir, in a sense, that faster the recycling, more is the enrichment of the reservoir (i.e. shorter the τ , more is the enrichment). They applied this hypothesis to the stratospheric ozone and showed that the same inverse relationship between τ and enrichment holds there for the existing data set. This helped them to predict an enrichment of about 140‰ at 40 km, knowing the decreasing trend of τ in the upper stratosphere (beyond 33 km). The stratospheric situation is, of course, not exactly similar to that of their experiment, but the basic process regulating the enhancement of fractionation should be similar.

Theoretical considerations

Previous studies

A significant number of theoretical studies have been made to explain the isotopic enrichment in ozone. However, until recently none could satisfactorily explain all the experimental observations. Most of these approaches are symmetry-based. Two types of point group symmetry (i.e. C_{2v} and C_s) exist for the ozone isotopomers and half of the rotational states are absent in the symmetric (C_{2v}) isotopomers. For ozone isotopomers $^{49}\text{O}_3$ and $^{50}\text{O}_3$, about one-third of all the molecules are symmetric (for example, $^{16}\text{O}^{18}\text{O}^{16}\text{O}$), and two-thirds are asymmetric (for example, $^{16}\text{O}^{16}\text{O}^{18}\text{O}$). Heidenreich and Thiemens⁴⁶ suggested that the asymmetric reaction intermediate in the $\text{O} + \text{O}_2$ collision has a longer lifetime than the symmetric reaction intermediate, which results in an efficient quenching of asymmetric species to ground-state ozone. Since the asymmetric species must involve the heavy isotopes, the product ozone is isotopically enriched.

Gellene⁴⁷ proposed a mechanism based on nuclear symmetry to model the observations. According to this approach, symmetry restriction arises for homonuclear diatomics ($^{16}\text{O}^{16}\text{O}$ and $^{18}\text{O}^{18}\text{O}$) involved in the $\text{O} + \text{O}_2$

collision because a fraction of their rotational states correlates with those of the corresponding ozone molecule. On the other hand, for heteronuclear molecules ($^{16}\text{O}^{18}\text{O}$), all of their rotational states correlate with those of the resulting ozone molecule. This model reproduces the general features of the observation of Krankowsky and Mauersberger⁴⁸, but cannot be satisfactorily applied for the other laboratory studies^{26,27,29}.

Non-statistical approach: A non-RRKM based model

In a series of recent publications^{49–53}, Marcus and co-workers (at CalTech) developed a model to explain the anomalous oxygen isotopic composition during ozone formation. Their work is based on the statistical theory developed by Rice, Ramsperger, Kassel and Marcus over a long period and is known as RRKM theory of unimolecular dissociation/bimolecular recombination in its vibrational form^{54–56}. It involves the formation of vibrationally excited ozone isotopomers from the recombination of O and O₂ through a hindered-rotor transition state.

In RRKM theory, for a bimolecular recombination, $X + YZ \rightarrow XYZ^*$ ('*' denoting a vibrationally excited molecule), the vibrational–rotational energy is supposed to be statistically distributed among its vibrational–rotational modes. This excited molecule can redissociate, $XYZ^* \rightarrow (X + YZ)$ or $(XY + Z)$ or lose its energy by collision to form a stable XYZ molecule. The unimolecular dissociation rate constant for a vibrationally excited molecule of vibrational–rotational energy E and total angular momentum J is given by,

$$k_{\text{EJ}} = N_{\text{EJ}}^+ / h\rho_{\text{EJ}} \quad (9)$$

N_{EJ}^+ is the number of quantum states accessible to the 'transition state' for dissociation for given E and J , and ρ_{EJ} is the density (number per unit energy) of quantum states of the vibrationally excited molecule.

In the new approach, this theory considers (i) the η -effect, which can be interpreted as a small deviation from the statistical density of states for symmetric isotopomers, compared with the asymmetric isotopomers; (ii) weak collisions for deactivation of the vibrationally excited ozone molecule, and (iii) a partitioning effect (Y -effect) which controls the recombination rate-constant ratios. The partitioning effect arises from small differences in zero-point energies of the two exit channels of dissociation of an asymmetric ozone isotopomer, which are magnified into large differences in the number of states in the two competing exit channel transition states. Considerations (i) and (iii) can be regarded as 'symmetry-driven' isotope effects. The above-mentioned points are briefly discussed below.

Non-statistical η -effect

As a modification of classical RRKM theory, it is argued that the effective ρ_{EJ} in eq. (9) might be less than the statistical value and more so for the symmetric isotopomers XXY^* than for XYZ^* . This ρ_{EJ} should only be the density of the quantum states of the triatomic molecule that are sufficiently dynamically coupled to the two exit channels, so that they can lead to the dissociation of the molecule in its typical lifetime. After the formation of the vibrationally excited molecule, the subsequent redistribution of energy among its vibrational–rotational modes at a given E and J proceeds at some finite rate and may be incomplete during the typical lifetime of the molecule (the non-RRKM effect). The ρ_{EJ} of eq. (9) should only refer to the quantum states which have been intramolecularly equilibrated. As there are fewer dynamical coupling terms in the symmetric XXY than in the asymmetric XYZ , some terms being forbidden by the symmetry, it was suggested that this non-RRKM effect for ρ_{EJ} is expected to be greater for XXY than for XYZ . The consequence of this nonstatistical effect is the nonmass-dependent isotopic fractionation.

The above description is shown pictorially in Figure 3 (after Gao and Marcus⁵²). During the typical lifetime of the dissociating ozone, the shaded regions indicate the ozone quantum states sufficiently strongly coupled dynamically to the exit channels so as to contribute to ρ_{EJ} during that lifetime. The shaded region for the asymmetric molecules is shown as a greater fraction of the total region than that of the symmetric molecules, since there are fewer coupling terms in the symmetric than in the asymmetric molecule. The ratio of the fraction of shaded to total region for the asymmetric molecule to the same fraction for the symmetric molecule is denoted by η .

Weak collisions for deactivation

During the stabilization of vibrationally hot molecule (XYZ^*), energy is transferred between excited ozone molecule and a bath gas molecule. The weak collision model assumes that the average energy lost by the vibrationally hot molecule (XYZ^*) in downward collisions and the energy gain in the upward collisions are relatively small. For simplicity, a step-ladder model, in which energy is transferred in discrete steps of ΔE per collision was considered.

Partitioning effect in dissociation channels

The reaction scheme of ozone formation includes a redissociation step consisting of two channels, (a) $XYZ^* \rightarrow X + YZ$, and (b) $XYZ^* \rightarrow XY + Z$, when $Z \neq X$. Due to the difference in zero-point energy of the product diatomic molecule, the rate constants of these two channels are

different and hence, the net bimolecular rate constant of the reaction $X + YZ \rightarrow XYZ$, is dependent on the dissociation channel it follows. So, the dissociation fate of XYZ^* is partitioned into two dissociation channels due to the zero point energy effect. This partitioning effect is denoted by Y ($\tilde{O}_a = N_{\text{EJ}}^{a+} / (N_{\text{EJ}}^{a+} + N_{\text{EJ}}^{b+})$ and $\tilde{O}_b = N_{\text{EJ}}^{b+} / (N_{\text{EJ}}^{a+} + N_{\text{EJ}}^{b+})$) in this model.

Interlink between RRKM-based theory and observed rate constants

With this non-statistical approach, Gao and Marcus⁵² tried to explain the results of different laboratory experiments^{28,29,31–33}. They observed that the calculated results of different experiments are sensitive to different model parameters (see table 1 of Gao and Marcus⁵²).

The calculated low-pressure rate constants at 300 K of individual channels for the formation of XYZ molecules (using $\eta = 1.18$ and $\Delta E = 210 \text{ cm}^{-1}$) agree well with that of the experimental value³³. The computed isotopic enrichment at low pressure for ‘scrambled’ systems, using these individual rate constants, also agrees with the experimental data of Mauersberger *et al.*³².

In view of the above experimental and theoretical studies, the observed anomalous isotopic fractionation in ozone can be explained by the sum of the effects arising out of different rate constants of different ozone-forming channels. We note that the Gao–Marcus model is restricted to the formation of ozone and does not consider photo-dissociation of ozone. However, the basic idea of departure from a statistical distribution of states can be useful in interpreting the results of photo-dissociation, where mass-independent character has been seen. The same departure from the statistical distribution can also be postulated during pure photo-dissociation of ozone, since a short-lived complex O_3^* is present as an intermediate during photo-dissociation of O_3 molecule (i.e. $\text{O}_3 + h\nu \rightarrow \text{O}_3^* \rightarrow \text{O}_2 + \text{O}$)⁴⁰.

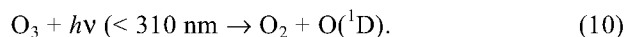
Ozone-induced anomalous composition in other stratospheric species

Photochemistry is the main driving force behind most of the reactions in the stratosphere. It initiates a large number of chemical cycles; the ozone cycle is one of the best examples. Photochemistry of ozone actively controls the chemistry of stratosphere and the isotopic distribution in oxygen containing trace gases due to exchange with ozone dissociation products. In the rest of this article we will discuss the oxygen isotopic composition of stratospheric CO_2 , an important stratospheric oxygen reservoir.

Oxygen isotopic composition of stratospheric CO_2

Gamo *et al.*⁵⁷ were the first to show that the $^{18}\text{O}/^{16}\text{O}$ ratio in stratospheric CO_2 is unusually high. Simultaneous de-

termination of $^{18}\text{O}/^{16}\text{O}$ and $^{17}\text{O}/^{16}\text{O}$ in stratospheric CO_2 (ref. 13) collected over Palestine, Texas and Fort Sumner, New Mexico at altitudes between 26 and 35.5 km showed enrichments varying from 7.9 to 12.6‰ and 10.0 to 15.5‰ in $\delta^{18}\text{O}$ and $\delta^{17}\text{O}$ respectively, compared to their tropospheric values (expressed as $\Delta\delta^{18}\text{O}$ and $\Delta\delta^{17}\text{O}$ hereafter). The average enrichment in ^{17}O ($\sim 11.8\text{‰}$) was slightly higher than that in ^{18}O ($\sim 10.5\text{‰}$). Interestingly, small but significant mass-independent signature ($\Delta^{17}\text{O} = \delta^{17}\text{O} - 0.52 \times \delta^{18}\text{O} = 0.11$ to 0.49) was also observed in CO_2 samples of upper troposphere collected between New Zealand and the South Pole at altitudes between 10.4 and 11.9 km (ref. 58). CO_2 collected over White Sands, New Mexico at much higher altitudes (between 29.3 and 60 km) showed $\Delta\delta^{18}\text{O}$ values from 4.1 to 14.5‰, with concomitant $\Delta\delta^{17}\text{O}$ ranging from 8.0 to 19.6‰ (ref. 14). Alexander *et al.*⁵⁹ performed the first simultaneous measurements of concentration of fluorinated compounds (SF_6 , CCl_3F (CFC-11), CCl_2F_2 (CFC-12), $\text{CCl}_2\text{FCClF}_2$ (CFC-113)) and the complete oxygen isotopic composition of CO_2 in the middle atmosphere (between 12 and 21 km). These data exhibit strong anti-correlation between the $\Delta^{17}\text{O}$ (the degree of mass-independent anomaly) and the CFC concentrations, which confirms that the mass-independent ($\Delta^{17}\text{O}$) signature of CO_2 serves as a good proxy for cross-transport and stratospheric residence times. Lämmerzahl *et al.*²⁴ recently re-confirmed the earlier measurements of stratospheric CO_2 (i.e. enrichment of heavy-oxygen isotopes) and demonstrated that the enrichment increases with altitude. Interestingly, they found that within the altitude range of 19 to 33 km, the enrichments in ^{17}O and ^{18}O (with maximum enrichments of about 8‰ in $\delta^{18}\text{O}$ and 13.5‰ in $\delta^{17}\text{O}$ with respect to tropospheric values) are linearly correlated with a slope ($d(\Delta\delta^{17}\text{O})/d(\Delta\delta^{18}\text{O})$) value close to 1.7. This slope value is relatively high compared to the previously obtained value of 1.2 from the upper stratospheric (above 40 km) measurements¹⁴. Yung *et al.*⁶⁰ first proposed that stratospheric ozone is the source of ‘heaviness’ of stratospheric CO_2 . The transfer of heaviness occurs via reaction of $\text{O}(^1\text{D})$ produced during UV photolysis of O_3 with CO_2 through an intermediate transient complex CO_3^* as follows:



During the atmospheric transport, tropospheric CO_2 molecules (as part of air-parcel) continuously ascend in the stratosphere and interact more and more with $\text{O}(^1\text{D})$ generated from local ozone photolysis. This results in continuous increase of isotopic enrichment of CO_2 with increasing altitude.

There are few experimental^{61,62} and theoretical^{16,63} efforts to understand the above exchange process. The

main problem in understanding the results is the unknown $O(^1D)$ composition, as one of the end members. Hence, it was not possible to clarify if this was a simple mixing process or a complex one involving the intermediate, CO_3^* , which can initiate unknown fractionation during its dissociation. However, measuring the oxygen isotopic composition of product oxygen after the photolysis of a mixture of CO_2 and O_3 (till all O_3 decomposed to O_2), Wen and Thiemens⁶¹ inferred that CO_2 – $O(^1D)$ exchange is an anomalous process. To model the stratospheric data (for both ^{17}O and ^{18}O in CO_2) of Zipf and Erdman⁶⁴, Barth and Zahn⁶³ considered that the $O(^1D)$ composition is same as that of ozone and modified it considering mass-dependent collisional rate with nitrogen (as an ambient gas). It was seen that an extra mass-dependent fractionation term has to be incorporated in the exchange process to match the real measurements. Johnston *et al.*⁶² tried to mimic the stratospheric condition by photolysing CO_2 and O_2 mixture of appropriate ratio, but were unsuccessful in measuring $\delta^{17}O$ of CO_2 (due to technical difficulties) and hence, could not discuss the stratospheric slope. However, their experiment with ‘high- CO_2 ’ (not similar to stratosphere) along with a numerical model study put forward some interesting aspects of this particular exchange process.

Recently, Chakraborty and Bhattacharya⁶⁵ studied the oxygen isotope exchange process between CO_2 and $O(^1D)$ (derived from UV photolysis of ozone). Photolysis of a mixture of CO_2 of nearly tropospheric composition (with $\delta^{17}O = 20.3\text{‰}$ and $\delta^{18}O = 39.3\text{‰}$) and O_3 of stratospheric (at 32 km altitude) composition (with $\delta^{17}O = 110\text{‰}$ and $\delta^{18}O = 124\text{‰}$ w.r.t. SMOW) was carried out for various periods (5 to 25 min) using UV light from a Hg resonance lamp. The experimental conditions were not exactly similar to those of stratosphere, since a large oxygen reservoir was missing. Nevertheless, they felt that the mechanism involved in the isotope transfer between these two stratospheric oxygen-bearing species (O_3 and CO_2) can be better understood if other interfering effects are absent. The results of this photolysis experiment show that the final CO_2 is enriched in both ^{17}O and ^{18}O , and the enrichments increase with time of exposure. It is also interesting to note that the enrichment in ^{17}O is always more than that in ^{18}O , and in a plot of $\delta^{17}O$ vs $\delta^{18}O$, the points fall on a line with a slope of 1.81. This slope value is close to that observed in the stratosphere²⁴, i.e. 1.71.

The importance of this work lies in the fact that they could estimate the isotopic composition of $O(^1D)$ generated by ozone photolysis. The isotopic composition of $O(^1D)$ was derived based on the assumption that only terminal atoms in the ozone molecule can be broken to form $O(^1D)$ during photo-dissociation of ozone. If ozone is isotopically enriched and the enrichment is mainly due to concentration of the heavy isotope in the asymmetric species, it is apparent that the $O(^1D)$ reservoir would

have enrichment higher than that of progenitor ozone, since asymmetry is caused by placement of a heavy isotope in the terminal position.

By analysing the experimental data through a model they also showed that the transfer of ‘heaviness’ from the ozone pool to the CO_2 pool in UV-induced exchange reaction cannot be explained by a simple mixing of CO_2 with $O(^1D)$ (which offers a slope value less than 1.28 instead of observed 1.81), but has a component due to fractionation from intermediate CO_3^* which favours ^{17}O transfer to CO_2 relative to ^{18}O . A fractionation mechanism involving singlet–triplet transition during dissociation of CO_3^* is proposed by Chakraborty and Bhattacharya⁶³ to account for their experimental observations. It is expected that similar mass-independent signature can be seen in all oxygen-bearing stratospheric species, which interact with $O(^1D)$.

Conclusion

An important area of research has evolved over the past decade involving anomalous mass-independent isotopic fractionation in extraterrestrial objects and stratospheric gases. The present article reviews some exciting recent developments in this field. In particular, mass-independent isotopic fractionation in stratospheric ozone and CO_2 is discussed and recent laboratory experiments as well as current theoretical models to account for these anomalous fractionations are described. Being a photochemically active species in the stratosphere, ozone plays a major role in controlling the oxygen isotopic distribution in oxygen-bearing stratospheric species. Moreover, ozone is a reservoir of mass-independent oxygen isotopic composition, and therefore, even a simple exchange process between $O(^1D)$ and other oxygen-bearing trace species (unlike the complex exchange process between CO_2 and $O(^1D)$) could potentially generate mass-independent isotopic composition in those exchanged molecules. The signature of mass independence offers a valuable tracer to understand many stratospheric processes.

1. Young, E. D. *et al.*, *Geochim. Cosmochim. Acta*, 2002, **66**, 1095–1104.
2. Thiemens, M. H., *Science*, 1999, **283**, 341–345.
3. Weston, Jr. R. E., *Chem. Rev.*, 1999, **99**, 2115–2136.
4. Clayton, R. N. *et al.*, *Science*, 1973, **182**, 485–488.
5. Huss, G. R. *et al.*, *Astrophys. J.*, 1994, **430**, L81–L84.
6. Hutcheon, I. D. *et al.*, *Astrophys. J.*, 1994, **425**, L97–L100.
7. Nittler, L. *et al.*, *Nature*, 1994, **370**, 443–446.
8. Mauersberger, K., *Geophys. Res. Lett.*, 1981, **8**, 935–937.
9. Mauersberger, K., *Geophys. Res. Lett.*, 1987, **14**, 80–83.
10. Mauersberger, K. *et al.*, *Geophys. Res. Lett.*, 2001, **28**, 3155–3158.
11. Schueler, B. *et al.*, *Geophys. Res. Lett.*, 1990, **17**, 1295–1298.
12. Krankowsky, D. *et al.*, *Geophys. Res. Lett.*, 2000, **27**, 2593–2595.
13. Thiemens, M. H. *et al.*, *Geophys. Res. Lett.*, 1991, **18**, 669–672.
14. Thiemens, M. H. *et al.*, *Science*, 1995, **270**, 969–972.

15. Rahn, T. and Wahlen, M., *Science*, 1997, **278**, 1776–1778.
16. Yung, Y. L. *et al.*, *J. Geophys. Res.*, 1997, **102**, 10,857–10,866.
17. Cliff, S. S. and Thieme, M. H., *Science*, 1997, **278**, 1774–1776.
18. Huff, A. K. and Thieme, M. H., *Geophys. Res. Lett.*, 1998, **25**, 3509–3512.
19. Röckmann, T. *et al.*, *Science*, 1998, **281**, 544–546.
20. Miller, M. F., *Geochim. Cosmochim. Acta*, 2002, **66**, 1881–1889.
21. DeMore, W. B. *et al.*, *Chemical Kinetics and Photochemical Data for Use in Stratospheric Modeling*, Evaluation Number 12, JPL Publication 97–26, 1997.
22. Anderson, S. M., Mauersberger, K. and Morton, J., in *Progress and Problems in Atmospheric Chemistry* (ed. Barker, J.), World Scientific, Singapore, 1995, pp. 473–499.
23. Stehr, J. *et al.*, *J. Atmos. Chem.*, 1996, **24**, 317–325.
24. Lämmerzahl, P. *et al.*, *Geophys. Res. Lett.*, 2002, **29**, 23–1–4.
25. Thieme, M. H. and Heidenreich, J. E., *Science*, 1983, **219**, 1073–1075.
26. Thieme, M. H. and Jackson, T., *Geophys. Res. Lett.*, 1987, **14**, 624–627.
27. Thieme, M. H. and Jackson, T., *Geophys. Res. Lett.*, 1988, **15**, 639–642.
28. Thieme, M. H. and Jackson, T., *Geophys. Res. Lett.*, 1990, **17**, 717–719.
29. Morton, J. *et al.*, *J. Geophys. Res.*, 1990, **95**, 901–907.
30. Mauersberger, K. *et al.*, *Geophys. Res. Lett.*, 1993, **20**, 1031–1034.
31. Anderson, S. M. *et al.*, *J. Chem. Phys.*, 1997, **107**, 5385–5391.
32. Mauersberger, K. *et al.*, *Science*, 1999, **283**, 370–372.
33. Janssen, C. *et al.*, *J. Chem. Phys.*, 1999, **111**, 7179–7182.
34. Janssen, C. *et al.*, *Phys. Chem. Chem. Phys.*, 2001, **3**, 4718–4721.
35. Chakraborty, S. and Bhattacharya, S. K., *Chem. Phys. Lett.*, 2003, **369**, 662–667.
36. Wen, J. and Thieme, M. H., *Chem. Phys. Lett.*, 1990, **172**, 416–420.
37. Wen, J. and Thieme, M. H., *J. Geophys. Res.*, 1991, **96**, 10,911–10,921.
38. Kim, S. and Yang, J., *J. Astron. Space Sci.*, 1997, **14**, 297–311.
39. Bhattacharya, S. K. and Thieme, M. H., *Geophys. Res. Lett.*, 1988, **15**, 9–12.
40. Chakraborty, S. and Bhattacharya, S. K., *J. Chem. Phys.*, 2003, **118**, 2164–2172.
41. Matsumi, Y. *et al.*, *J. Chem. Phys.*, 2002, **107**, ACH 1–1–12.
42. Chakraborty, S. and Bhattacharya, S. K., Proc. First International Symposium on Isotopomers (ISI 2001), Yokohama, Japan, 2001, ISI2001–15.pdf.
43. Irion, F. W. *et al.*, *Geophys. Res. Lett.*, 1996, **23**, 2377–2380.
44. Meier, A. and Notholt, J., *Geophys. Res. Lett.*, 1996, **23**, 551–554.
45. Bhattacharya, S. K. *et al.*, *J. Geophys. Res.*, 2002, **107**, 4675.
46. Heidenreich, III J. E. and Thieme, M. H., *J. Chem. Phys.*, 1986, **84**, 2129–2136.
47. Gellene, I. G., *Science*, 1996, **274**, 1344–1346.
48. Krankowsky, D. and Mauersberger, K., *Science*, 1996, **274**, 1324–1325.
49. Hathorn, B. C. and Marcus, R. A., *J. Chem. Phys.*, 1999, **111**, 4087–4100.
50. Hathorn, B. C. and Marcus, R. A., *J. Chem. Phys.*, 2000, **113**, 9497–9509.
51. Marcus, R. A. and Gao, Y. Q., *J. Chem. Phys.*, 2001, **114**, 9807–9812.
52. Gao, Y. Q. and Marcus, R. A., *Science*, 2001, **293**, 259–262.
53. Gao, Y. Q. and Marcus, R. A., *J. Chem. Phys.*, 2002, **116**, 137–154.
54. Marcus, R. A., *J. Chem. Phys.*, 1952, **20**, 352–354.
55. Marcus, R. A., *J. Chem. Phys.*, 1952, **20**, 355–358.
56. Marcus, R. A., in *Chemische Elementarprozesse* (ed. Hartmann, H.), Springer-Verlag, New York, 1968, p. 348.
57. Gamo, T. *et al.*, *Tellus*, 1989, **B41**, 127–133.
58. Thieme, M. H. *et al.*, *Geophys. Res. Lett.*, 1995, **22**, 255–257.
59. Alexander, B. *et al.*, *Geophys. Res. Lett.*, 2001, **28**, 4103–4106.
60. Yung, Y. L. *et al.*, *J. Geophys. Res.*, 1991, **18**, 13–16.
61. Wen, J. and Thieme, M. H., *J. Geophys. Res.*, 1993, **98**, 12,801–12,808.
62. Johnston, J. C. *et al.*, *J. Geophys. Res.*, 2000, **105**, 15,213–15,229.
63. Barth, V. and Zahn, A., *J. Geophys. Res.*, 1997, **102**, 12,995–13,007.
64. Zipf, E. C. and Erdman, P. W., NASA's Upper Atmosphere Research Programme (UARP) and Atmospheric Chemistry Modeling and Analysis Programme (ACMAP) Research Summaries 1992–1993, Report to Congress and Environmental Protection Agency, 1994.
65. Chakraborty, S. and Bhattacharya, S. K., *J. Geophys. Res.* (revised version submitted for acceptance), 2002.

Received 25 September 2002; revised accepted 5 December 2002